

Figure S2. **Specificity of antibodies to ELKS1, ELKS2, and bMunc13-2.** (A–C) Immunohistochemical analyses of the dentate gyrus of control (top) and the indicated KO mice (bottom) with anti-ELKS1 (A), anti-ELKS2 (B), and anti-bMunc13-2 (C) antibodies. All sections were counterstained for Bassoon as a marker of AZs. Most ELKS1, ELKS2, and bMunc13-2 signals were eliminated in the corresponding KOs. Note that signals for ELKS1 and bMunc13-2 are enriched in the hilus and colocalize with a limited fraction of Bassoon-positive structures, whereas most ELKS2 signals colocalize with Bassoon-positive structures. Bars, 50  $\mu$ m.



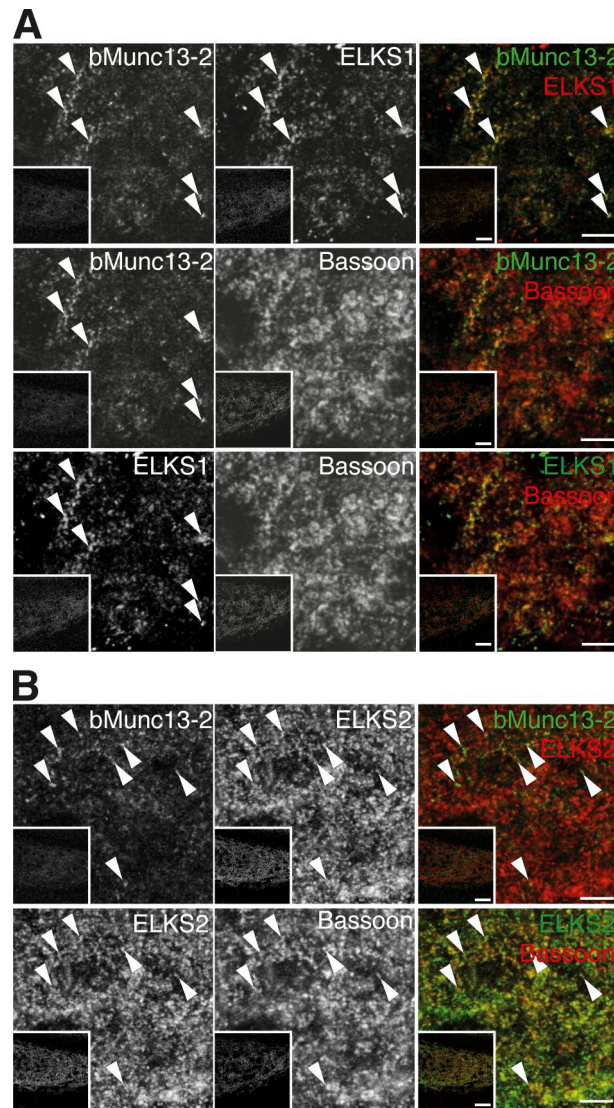


Figure S3. **Preferential recruitment of bMunc13-2 to ELKS1 enriched synapses in the hippocampus.** (A and B) Localization of endogenous bMunc13-2, ELKS1, and Bassoon (A) and of bMunc13-2, ELKS2, and Bassoon (B) in the WT mouse hippocampus (hilus of the dentate gyrus). Note that bMunc13-2 shows a distribution pattern similar to that of ELKS1 with a restriction to a limited number of synapses (arrowheads), whereas ELKS2 is accumulated in most Bassoon-positive AZs (B). Bars: (low-magnification insets) 50  $\mu$ m; (high magnification) 5  $\mu$ m.



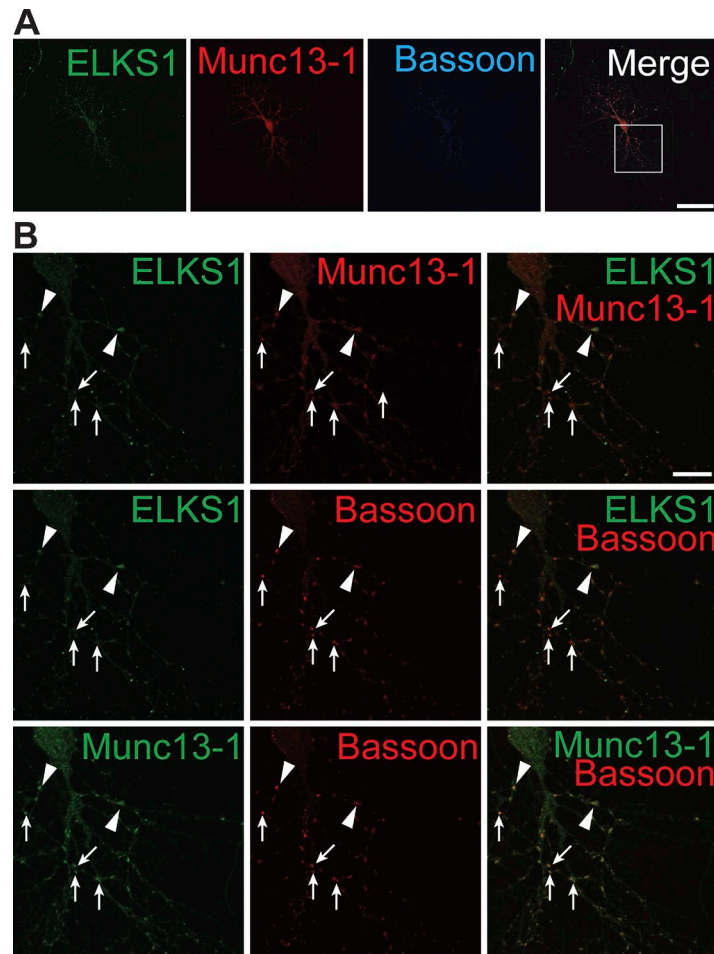


Figure S4. **Neuronal distribution of ELKS1, Munc13-1, and Bassoon.** Autaptic primary cultured neurons immunostained with antibodies to ELKS1, Munc13-1, and Bassoon. (A) Low-power image of an entire autaptic neuron showing that Munc13-1-containing synapses (red) are more abundant than ELKS1-containing synapses (green). Bar, 50  $\mu$ m. (B) High-power image of boxed region in A. Some synapses show enriched ELKS1 levels (arrowheads), whereas most of them contain no or very little ELKS1 (arrows). Overall,  $\sim 14\%$  of Munc13-1 and Bassoon double-positive puncta appeared to accumulate ELKS1 ( $n = 960$  synapses,  $n = 12$  neurons). Bar, 10  $\mu$ m.



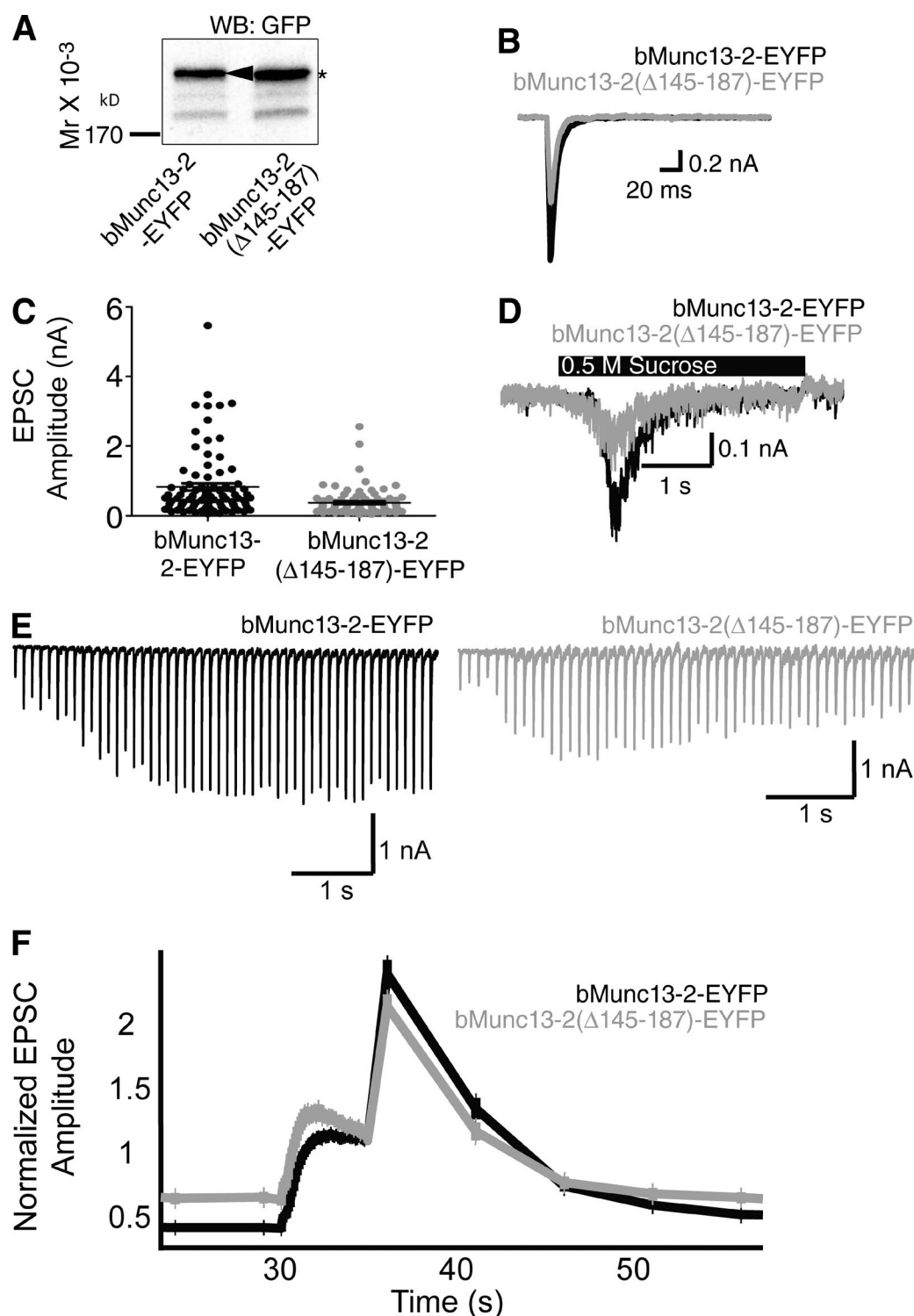


Figure S5. **Rescue of Munc13-1/2 DKO neurons by reexpression of WT of ELKS1-binding-deficient mutant of bMunc13-2.** (A) Expression levels of bMunc13-2-EYFP and bMunc13-2(Δ145-187)-EYFP proteins upon Semliki Forest virus infection. Relative protein levels of bMunc13-2-EYFP (arrowhead) versus bMunc13-2(Δ145-187)-EYFP (asterisk), as assessed by densitometric analysis of bands on films (ImageJ) and normalized to infection efficiencies, were 1:1.23. WB, Western blot. (B) Example traces of evoked EPSCs from neurons expressing bMunc13-2-EYFP (black) or bMunc13-2(Δ145-187)-EYFP (gray) in response to a single action potential. (C) Scatterplots of EPSC amplitudes from Munc13-1/2 DKO neurons expressing bMunc13-2-EYFP (black dots) or bMunc13-2(Δ145-187)-EYFP (gray dots). Data from neurons that did not show responses were not included. (D) Example traces of evoked EPSCs induced by 0.5 M sucrose from neurons expressing bMunc13-2-EYFP (black) or bMunc13-2(Δ145-187)-EYFP (gray). (E) Example traces of evoked EPSCs from neurons expressing bMunc13-2-EYFP (black) or bMunc13-2(Δ145-187)-EYFP (gray) during a 10-Hz action potential train. (F) Time course of short-term plasticity (10-Hz stimulus train at 30–35 s) of Munc13-1/2 DKO neurons expressing bMunc13-2-EYFP (black,  $n = 87$ ) or bMunc13-2(Δ145-187)-EYFP (gray,  $n = 83$ ). Evoked EPSCs were normalized to the levels at the end of the 10-Hz action potential trains. Note that the time courses of facilitation and augmentation of EPSCs are almost identical between Munc13-1/2 DKO neurons expressing bMunc13-2-EYFP (black) and bMunc13-2(Δ145-187)-EYFP (gray).